HHS Public Access

Author manuscript

Nat Immunol. Author manuscript; available in PMC 2016 October 11.

Published in final edited form as:

Nat Immunol. 2016 June ; 17(6): 704–711. doi:10.1038/ni.3438.

Asymmetric inheritance of mTORC1 kinase activity during division dictates CD8 T cell differentiation

Kristen N. Pollizzi[1,2,*], **Im-Hong Sun**[1,*], **Chirag H. Patel**[1,*], **Ying-Chun Lo**[1,3], **Min-Hee Oh**[1], **Adam T. Waickman**[1,4], **Ada J. Tam**[1], **Richard L. Blosser**[1], **Jiayu Wen**[1], **Greg M. Delgoffe**[1,5], and **Jonathan D. Powell**[1]

[1]Sidney-Kimmel Comprehensive Cancer Research Center, Department of Oncology, Johns Hopkins University School of Medicine, Baltimore, Maryland, USA

[5]Department of Immunology, University of Pittsburgh, Pittsburgh, Pennsylvania, USA

Abstract

The asymmetric partitioning of fate determining proteins has been shown to contribute to the generation of effector and memory CD8$^+$ T cell precursors. Here, we demonstrate the asymmetric partitioning of mTORC1 activity upon activation of naïve CD8$^+$ T cells. This results in the generation of one daughter T cell with increased mTORC1 activity, increased glycolytic activity and increased expression of effector molecules. The other daughter T cell inherits relatively low levels of mTORC1 activity, possesses increased lipid metabolism, expresses increased anti-apoptotic molecules and subsequently displays enhanced long-term survival. Mechanistically, we demonstrate a link between TCR-induced asymmetric expression of amino acid transporters and RagC-mediated translocation of mTOR to the lysosomes. Overall, our data provide important insight into how mTORC1-mediated metabolic reprogramming affects the fate decisions of T cells.

Asymmetric division is an evolutionarily conserved mechanism by which a single cell gives rise to two daughter cells of distinct fates [1]. The asymmetric partitioning of fate determining proteins has been shown to contribute to the generation of effector and memory CD8$^+$ T cell precursors based on differing levels of CD8 expression (CD8^{hi} and CD8^{lo}) [2,3]. Previous work has identified that CD8^{hi} T cells are derived from the daughter cell proximal to the antigen presenting cell (APC) and ultimately differentiate into effector CD8$^+$ T cells; in

Correspondence to: Jonathan D. Powell, ; Email: poweljo@jhmi.edu

[2]Present Address: Department of Research Oncology, MedImmune LLC, Gaithersburg, Maryland, USA.

[3]Present Address: Department of Pathology, Yale School of Medicine, New Haven, Connecticut, USA.

[4]Present Address: Experimental Immunology Branch, National Cancer Institute, NIH, Bethesda, Maryland, USA.

[*]Contributed equally and should be considered co-first authors

Competing financial interests

The authors declare no competing financial interests.

Contributions

K.N.P., I.-H.S., C.H.P., and J.D.P planned the experiments, analyzed the data and wrote the manuscript, K.N.P., I.-H.S., C.H.P., Y.-C.L, M.-H.O., A.T.W and J.W. performed the experiments; G.M.D and A.T.W. contributed to the experimental design, execution and data interpretation; A.J.T. and R.L.B. provided support for flow cytometry experiments; G.M.D. and J.D.P conceived the idea for the study; K.N.P., I.-H.S., C.H.P., Y.-C.L, M.-H.O., G.M.D and J.D.P provided critical review of the manuscript.

contrast, $CD8^{lo}$ T cells are derived from the daughter cell distal to the APC and give rise to $CD8^+$ memory T cells [2–5]. Subsequent studies have further demonstrated asymmetry in critical transcription factors such as T-bet and TCF-1 in mediating the phenotypic differences between daughter cells [3,6].

The mTOR signaling pathway plays a critical role in regulating $CD4^+$ T cell activation and differentiation [7–12] as well as regulating $CD8^+$ T cell effector and memory generation [13–17]. In part, the ability of mTOR to coordinate T cell differentiation and activation has been attributed to its ability to promote metabolic reprogramming [18–20]. Robust mTORC1 activity promotes glycolytic activity and increased expression of effector molecules in $CD8^+$ T effector cells [16]. Indeed, T-*Tsc2*$^{-/-}$ $CD8^+$ T cells, which display hyperactive mTORC1 activity, demonstrate enhanced cytotoxic T lymphocyte (CTL) activity but fail to develop into persistent memory T cells. Alternatively, antigen stimulation in the presence of the mTORC1 inhibitor rapamycin leads to enhanced generation of memory T cells, and $CD8^+$ T cells with diminished mTORC1 activity derive energy utilizing fatty acid oxidation rather than glycolysis [13–16].

Here we tested the hypothesis that mTORC1 activity is asymmetrically inherited upon the first cell division of naïve $CD8^+$ T cells. We demonstrate the asymmetric partitioning of mTORC1 activity upon activation of $CD8^+$ T cells. This results in the generation of one daughter T cell with relatively increased mTORC1 activity, glycolytic activity, and expression of effector molecules. The other daughter T cell inherits relatively low levels of mTORC1 activity, possesses increased spare respiratory capacity (SRC) and lipid metabolism, expression of anti-apoptotic molecules and subsequently displays enhanced long-term survival. Mechanistically, we demonstrate a link between TCR-induced asymmetric expression of amino acid transporters and RagC-mediated translocation of mTOR to the lysosomes. Overall, our data provide important insight into how mTORC1-mediated metabolic reprogramming affects the fate decisions of $CD8^+$ T cells.

Results

Divided $CD8^+$ T cells possess asymmetric mTORC1 kinase activity

To determine if mTORC1 activity is asymmetrically inherited during cellular division, cells from mice with transgenic expression of major histocompatibility (MHC) class I-restricted (ovalbumin specific) TCR (OT-I) were labeled with cell proliferation dye-eFluor450 (eFluor450) and were intravenously (i.v.) transferred into C57BL/6 wild-type hosts. The next day, these mice were infected with *Listeria monocytogenes* expressing ovalbumin (LM-OVA) (i.v.) and splenocytes were harvested 48 h later. Consistent with previous studies [2–4,21], when examining $CD8^+$ T cells from the first division (second brightest eFlour450 population), we observed two distinct populations based on CD8 surface expression, cells with high CD8 expression (hereafter $CD8^{hi}$) and low CD8 expression (hereafter $CD8^{lo}$) (Fig. 1a). Similarly, when comparing these two populations, we observed higher expression of CD25 and T-bet in the $CD8^{hi}$ T cells while the $CD8^{lo}$ T cells have higher expression of CD62L (Fig. 1a). Assessment of mTORC1 activity by flow cytometry based on phosphorylation of downstream target ribosomal S6 (p-S6) revealed that the $CD8^{hi}$

T cells had enhanced p-S6 expression compared to the $CD8^{lo}$ T cells, suggesting increased mTORC1 activity in the $CD8^{hi}$ T cells (Fig. 1a).

To confirm if differential inheritance of CD8 expression and mTORC1 activity is a consequence of cellular division or occurs prior to division, we compared expression levels in $CD8^+$ T cells from the first division with undivided counterparts (brightest eFlour450 population). Undivided T cell expressed lower levels of CD8 than cells from the first division (Supplementary Fig. 1a), indicating that heterogeneous expression of CD8 is induced after cellular division. Likewise, upon the first division, but not in the undivided population, we observed distinct populations of T cells heterogeneous for p-S6, CD98 and T-bet expression (Supplementary Fig. 1b), suggesting two distinct populations of T cells emerging only after first division, and independent of CD8 expression within the undivided T cell population. Unlike T-bet, Eomesodermin (Eomes), a transcription factor essential for both $CD8^+$ T effector and memory cells [22], was not asymmetrically distributed during the first division (Supplementary Fig. 1c), and both $CD8^{hi}$ and $CD8^{lo}$ T cell populations from the first division had higher expression of CD44 than naïve $CD8^+$ T cells (Supplementary Fig. 1c), indicating that both populations were equally activated and not all proteins were asymmetrically inherited.

Next, we sought to determine whether the *in vivo* findings could be validated with an *in vitro* system using carboxyfluorescein succinimidyl ester (CFSE) labeled OT-I $Rag2^{-/-}$ splenocytes stimulated with ovalbumin MHC class I peptide (OVA-I). Consistent with our earlier finding (Fig. 1a), $CD8^{hi}$ T cells displayed higher p-S6 compared to $CD8^{lo}$ T cells (Fig. 1b). Similarly, phosphorylation of 4E-BP1, another downstream substrate of mTORC1, was also highly expressed in $CD8^{hi}$ T cells compared to $CD8^{lo}$ T cells (Fig. 1b). While both $CD8^{hi}$ and $CD8^{lo}$ T cells had similar expression of TSC2, a negative regulator of mTORC1 activity, expression of phosphorylated TSC2 was found higher in $CD8^{hi}$ T cells compared to $CD8^{lo}$ T cells (Fig. 1b), indicating a reduced inhibition of mTORC1 activity in $CD8^{hi}$ T cells.

To further confirm these results, we sorted *in vitro* generated $CD8^{hi}$ and $CD8^{lo}$ T cells to assess mTOR activity by immunoblotting. $CD8^{hi}$ T cells had increased p-S6, but no significant difference in phosphorylation of AKT, a downstream target of mTORC2, compared to $CD8^{lo}$ T cells (Fig. 1c). Compared to $CD8^{lo}$ T cells, $CD8^{hi}$ T cells also had higher phosphorylation of 4E-BP1, but expressed equivalent amounts of phosphorylated ERK (Supplementary Fig. 1d), suggesting the differences in signaling are selective for the mTORC1 pathway. Both the $CD8^{hi}$ and $CD8^{lo}$ daughter T cells showed increased expression of the activation-induced markers CD69 and CD44 (Supplementary Fig. 1e), suggesting that the differences in mTORC1 signaling are not due to lack of TCR activation.

We next assessed the partitioning of proteins in dividing T cells by confocal microscopy using an *in vitro* system with plate-bound anti-CD3, anti-CD28 and ICAM-1, which has previously been shown to induce $CD8^+$ T cells asymmetric division [2,3]. Both daughter $CD8^+$ T cells displayed roughly equivalent amounts of S6 protein (Fig. 1d). However, the ratio between the mean fluorescence intensity (MFI) of p-S6 over total S6 was higher in $CD8^{hi}$ T cells compared to $CD8^{lo}$ T cells (Fig. 1d), indicating increased mTORC1 activity in $CD8^{hi}$ T

cells. To control that these results are not skewed by a minor subpopulation displaying great asymmetry of mTORC1 activity, we quantified the frequency of dividing $CD8^+$ T cells that asymmetrically partition p-S6 at first division to be 60% (see methods) (Fig. 1e), which is comparable with the frequency of T cell reported to undergo asymmetric distribution of T-bet (66%) [3]. As a control, we observed no asymmetric partitioning of β-tubulin and CD90.2 between dividing $CD8^+$ daughter T cells (Fig. 1e).

As previous studies have indicated that the interaction of LFA-1 on T cells with ICAM-1 on APCs (or plate-bound stimulation) is required for the asymmetric division of $CD8^+$ T cells [2,3,5,23], we tested whether the asymmetric partitioning of mTORC1 activity was a consequence of polarity. Confocal imaging of a dividing T cell pair in contact with an APC indicated increased p-S6 in the proximal daughter T cell compared to the distal T cell (Supplementary Fig. 1f). To test whether non-polarized T cell division, such as during homeostatic T cell proliferation in the absence of antigen stimulation, would result in non-asymmetric inheritance of mTORC1 activity in daughter T cells, labeled OT-I T cells were adoptively transferred (i.v.) into *Rag2*$^{-/-}$ mice. Seventy-two hours later, we observed a relatively uniform distribution of CD8 expression on the transferred T cells that had undergone the first division, as opposed to the bimodal peaks of CD8 expression observed during antigen-induced (polarized) activation (Fig. 1f). Furthermore, none of the transferred $CD8^+$ T cells recovered from the *Rag2*$^{-/-}$ recipients demonstrated differential expression of p-S6, CD25, CD62L, T-bet, MYC or CD98 within the first division, in contrast to T cells undergoing antigen-induced division during a LM-OVA infection (Fig. 1f and data not shown). Thus, asymmetric partitioning of mTORC1 activity in $CD8^+$ T cells is not a generalized property of cell division but rather of APC-antigen-driven (polarized) activation.

To determine whether asymmetric cell division is dependent upon mTORC1 activity, we compared *in vitro* activated wild-type $CD8^+$ T cells, T-*Rheb*$^{-/-}$ $CD8^+$ T cells, which have markedly decreased mTORC1 activity, and T-*Tsc2*$^{-/-}$ $CD8^+$ T cells, which have hyper-active mTORC1 activity. Using confocal microscopy, dividing daughter cells were identified via the tubulin bridge. Similar to wild-type $CD8^+$ T cells, $CD8^{hi}$ and $CD8^{lo}$ daughter pairs were found in dividing T-*Rheb*$^{-/-}$ and T-*Tsc2*$^{-/-}$ $CD8^+$ T cells (Fig. 1g), indicating that asymmetric division of CD8 expression is not controlled by mTORC1 activity. Furthermore, we observed no asymmetric partitioning of p-S6 in dividing T-*Rheb*$^{-/-}$ and T-*Tsc2*$^{-/-}$ $CD8^+$ T cells compared to wild-type $CD8^+$ T cells, thereby showing that differential mTORC1 activity in dividing T cells is required for asymmetric partitioning of mTORC1 activity to occur. Overall, these results so far indicate that mTORC1 activity is divided asymmetrically in the $CD8^{hi}$ and $CD8^{lo}$ daughter T cells during the first antigen-driven cell division.

Asymmetric mTORC1 activity promotes distinct metabolic programs

mTORC1 plays an important role in regulating the metabolic reprogramming of T cells, which in turn regulates T cell fate and function [19]. To test whether the asymmetric partitioning of mTORC1 activity would lead to the generation of two daughter $CD8^+$ T cells with distinct metabolic profiles, we compared the metabolic phenotype of sorted $CD8^{hi}$ and $CD8^{lo}$ T cells generated under *in vitro* activation. $CD8^{hi}$ T cells showed a higher basal and maximal extracellular acidification rate (ECAR) compared to $CD8^{lo}$ cells (Fig. 2a),

indicative of increased glycolysis and consistent with the current view that $CD8^+$ effector T cells are highly glycolytic [18]. Alternatively, we observed that the $CD8^{lo}$ T cells have higher SRC (Fig. 2b), a metabolic feature of long-lived cells [18,24,25], compared to $CD8^{hi}$ T cells.

MYC plays an important role in the metabolic reprogramming of both $CD4^+$ and $CD8^+$ T cells upon TCR activation, especially controlling the expression of multiple glycolytic enzymes [26], and MYC expression is enhanced by mTORC1 activation [27,28]. To test if MYC was preferentially upregulated in $CD8^{hi}$ T cells compared to $CD8^{lo}$ T cells, we adoptively transferred (i.v.) labeled OT-I T cells into wild-type hosts that were then infected with LM-OVA (i.v.). Upon flow cytometric assessment of $CD8^{hi}$ and $CD8^{lo}$ T cells from the first division, MYC protein was asymmetrically enriched in the $CD8^{hi}$ T cells compared to $CD8^{lo}$ T cells (Fig. 2c). Similarly, upon *in vitro* stimulation, asymmetric partitioning of MYC was observed by immunoblot analysis of sorted $CD8^{hi}$ and $CD8^{lo}$ T cells (Fig. 2d) and by confocal microscopy of $CD8^{hi}$ and $CD8^{lo}$ T cell dividing daughter pairs (Fig. 2e). In addition to MYC, $CD8^{hi}$ T cells also showed higher expression of hexokinase 2 (HK2) and GLUT-1, which are key proteins involved in the glycolytic pathway, compared to $CD8^{lo}$ T cells (Fig. 2d). Overall, our data demonstrate that upon $CD8^+$ T cell division, the asymmetric partitioning of mTORC1 activity is associated with the generation of $CD8^{hi}$ $mTOR^{hi}$ MYC^{hi} T cells that are highly glycolytic.

$CD8^{lo}$ daughter T cells generated by the asymmetric division contribute to the generation of memory $CD8^+$ T cells [2,4], which have distinct metabolic and mitochondrial profiles compared to effector $CD8^+$ T cells [14,24,25]. To further assess the metabolic reprogramming of $CD8^{lo}$ T cells, we examined the relative mitochondrial content of these cells compared to the highly glycolytic $CD8^{hi}$ T cells from sorted *in vitro* generated T cells. $CD8^{lo}$ T cells had a higher mitochondrial to genomic DNA ratio compared to $CD8^{hi}$ T cells (Fig. 2f). In addition, by confocal microscopy, we observed increased mitochondrial mass in sorted $CD8^{lo}$ T cells compared to $CD8^{hi}$ T cells (Fig. 2g). Furthermore, immunoblot analysis of sorted *in vitro* generated $CD8^{lo}$ T cells also showed increased expression of the mitochondrial protein VDAC as well as proteins associated with oxidative phosphorylation (NDUFB8 and SDHA), and pro-survival proteins (BCL-2 and BCL-xL) compared to $CD8^{hi}$ T cells (Fig. 2h). In addition, CPT-1α, an enzyme that is critical in fatty acid oxidation and enriched in memory $CD8^+$ T cells [14,24,25], was increased in $CD8^{lo}$ T cells compared to $CD8^{hi}$ T cells (Fig. 2h). Thus, while $CD8^{lo}$ T cells have decreased glycolysis, their increase in lipid metabolism and SRC is associated with an increase in mitochondrial mass and function that are critical in memory T cell formation [14,24,25].

$CD8^{lo}$ daughter T cells become long-lived memory T cells

Next, we investigated if asymmetric partitioning of mTORC1 activity correlated with distinct immune function. Consistent with previous findings [2,4], sorted *in vitro* activated $CD8^{hi}$ T cells expressed increased levels of IFN-γ (*Ifng*) and perforin (*Prf1*) mRNA as assessed by qRT-PCR (Supplementary Fig. 1g). As measured by ELISA, sorted $CD8^{hi}$ T cells produced more IFN-γ than $CD8^{lo}$ T cells (Supplementary Fig. 1h). Next, to evaluate the impact of asymmetric mTORC1 activation on $CD8^+$ T cells survival, we adoptively transferred (i.v.) congenically-marked sorted *in vitro* activated $CD8^{hi}$ or $CD8^{lo}$ T cells into

wild-type hosts that were infected with vaccinia-OVA either the same day or 21 days after transfer. Upon assessment of splenocytes six days after the adoptive transfer, we detected similar numbers of antigen specific $CD8^+$ T cells from the mice that received $CD8^{hi}$ or $CD8^{lo}$ T cell populations (Fig. 3a). However, $CD8^{hi}$ T cells were barely detectable after re-challenge *in vivo* at 21 days post-adoptive transfer (Fig. 3b), indicating that transferred $CD8^{hi}$ T cells failed to differentiate into proper memory T cells. In contrast, $CD8^{lo}$ T cells were able to persist and respond to secondary challenge (Fig. 3b). In addition, naïve $CD8^+$ T cells stimulated non-specifically with PMA and ionomycin, which induce non-polarized cell division, resulted in symmetrical high mTORC1 activity between $CD8^{hi}$ and $CD8^{lo}$ T cells (Supplementary Fig. 2), and also showed decreased memory formation *in vivo* in response to secondary challenge (Fig. 3b). These observations suggest that $CD8^{hi}$ T cells possess robust effector function but fail to survive and thus are not detected upon re-challenge, whereas $CD8^{lo}$ cells initially possess reduced effector capacity, but survive and proliferate upon re-challenge.

T cell activation leads to translocation of mTOR to the lysosome

We sought to define the cellular mechanism that accounts for the asymmetric partitioning of mTORC1 activity upon the first division in $CD8^+$ T cells. Amino acid sufficiency has been shown to promote mTORC1 localization to the lysosomal surfaces, where mTORC1 can become activated [29,30]. This occurs through the activation of the Rag GTPases, which upon amino acid sensing, disassociate from the lysosomal surface to capture mTOR in the cytoplasm and then shuttle back to the lysosomes [29,31]. TCR-mediated activation in $CD8^+$ T cells is known to elevate amino acid uptake [32], thus, we tested whether TCR activation regulates the ability of the Rag GTPases to promote the translocation of mTOR to the lysosomes. We stimulated naïve OT-I $CD8^+$ T cells with OVA-I peptide *in vitro* for 0, 4 or 24 hours and assessed the co-localization of RagC (a member of the Rag GTPases) and the lysosome marker LAMP-2 by confocal microscopy. Upon four hours of T cell activation, there was an initial decrease in the association of RagC and LAMP-2 compared to unstimulated T cells (Fig. 4a), indicating that TCR stimulation leads to the translocation of RagC from the lysosomes to the cytoplasm. By 24 hours post-activation, RagC partially re-localized to the lysosomes (Fig. 4a).

Next, we used confocal microscopy to determine the movement of mTOR to the lysosomes. Assessment of co-localization of mTOR and LAMP-2 in naïve unstimulated $CD8^+$ T cells indicated minimal mTOR localization to the lysosomes; however, as early as four hours after antigen stimulation, mTOR co-localized with the lysosomes and this association further increased at 24 hours (Fig. 4b). We observed a similar increase of mTOR translocation to the lysosomes in T-$Rheb^{-/-}$ and T-$Tsc2^{-/-}$ $CD8^+$ T cells as wild-type $CD8^+$ T cells (Fig. 4c), indicating that translocation of mTOR to the lysosomes is independent of mTORC1 activity. Our data thus far establishes that TCR activation of $CD8^+$ T cells initiates the translocation of mTOR to the lysosome.

To determine if mTOR localization to the lysosomes was observed in asymmetrically dividing $CD8^+$ T cells, we performed confocal microscopy on *in vitro* activated T cells undergoing division. We observed increased co-localization of mTOR and LAMP-2 in

CD8^{hi} T cells compared to CD8^{lo} T cells (Fig. 4d). These observations suggest that asymmetric inheritance of mTORC1 activity occurs as the result of the preferential translocation of mTOR to the lysosomes in the CD8^{hi} T cell compared to the CD8^{lo} T cell.

CD98 expression levels lead to asymmetric mTOR localization

We next investigated the mechanism accounting for the increased translocation of mTOR to the lysosomes in CD8^{hi} T cells. RagC-mediated translocation of mTOR to the lysosomes is induced by amino acid influx (particularly the branch chain amino acid leucine) [29]. To test whether differential mTORC1 activity among daughter T cells may be the result of the asymmetric partitioning of amino acid transporters upon cell division and differential leucine influx, we assessed the expression of the amino acid transporter SLC7A5, which controls leucine influx and subsequent mTORC1 activation, and as such has an essential role in CD8^{+} effector T cell generation [32]. We observed increased expression of *Slc7a5* mRNA in sorted *in vitro* generated CD8^{hi} T cells compared to CD8^{lo} T cells by qRT-PCR (Fig. 5a).

To explore if the leucine amino acids transporter was preferentially upregulated in CD8^{hi} T cells compared to CD8^{lo} T cells, we adoptively transferred (i.v.) labeled OT-I T cells into WT hosts that were infected with LM-OVA (i.v.) 24 hours later. As reliable detection of SLC7A5 protein is currently unavailable, we instead assessed the expression of CD98, a glycoprotein that forms a heterodimer with SLC7A5 [33]. Flow cytometric observation of CD8^{hi} and CD8^{lo} T cells determined that CD98 expression was asymmetrically enriched in the CD8^{hi} T cells compared to CD8^{lo} T cells (Fig. 5b). Additionally, upon *in vitro* activation, we observed higher CD98 expression on dividing CD8^{hi} than CD8^{lo} T cells by confocal microscopy (Fig. 5c). This implies that CD98 is asymmetrically partitioned between dividing daughter CD8^{+} T cells.

Consistent with published findings [34], co-culture of OT-I CD8^{+} T cells with peptide-loaded bone marrow derived APCs induced the CD98 localization at the immunological synapse, as indicated by co-localization with talin (Supplementary Fig. 3). Because CD98 interacts with ICAM-1 to facilitate leucine uptake [34], we tested whether CD98, along with SLC7A5, was preferentially enriched in the CD8^{hi} T cell compared to CD8^{lo} T cell. We observed that in dividing T cell pairs, the daughter T cells with higher CD98 expression had greater co-localization of mTOR to the lysosomes than the daughter T cells with lower CD98 expression (Fig. 5d). Of note, T-*Rheb*$^{-/-}$ CD8^{+} T cells displayed asymmetric inheritance of CD98 (Supplementary Fig. 4), indicating that mTORC1 does not control the asymmetric distribution of CD98 during division (note though, they showed lower expression of CD98 than wild-type CD8^{+} T cells).

Next, we tested the functional consequences of inhibiting SLC7A5 on TCR-induced mTOR translocation. *In vitro* activation of naïve CD8^{+} T cells in the presence of the amino acid transport inhibitor 2-aminobicyclo-(2,2,1)-heptane-2-carboxylic acid (BCH) led to decreased p-S6 in CD8^{+} T cells compared to untreated T cells but similar to expression in the unstimulated T cells (Fig. 5e). However, we observed no difference in CD98 expression in activated CD8^{+} T cells between the untreated and BCH-treated condition (Fig. 5e). Likewise, inhibition of SLC7A5 activity with BCH during CD8^{+} T cell activation led to decreased translocation of mTOR to the lysosome compared to the untreated condition (Fig.

5f). In contrast, rapamycin treatment, which inhibits mTORC1 activity independent of amino acid influx, had no effect on mTOR translocation to the lysosome in TCR-activated $CD8^+$ T cells (Fig. 5f), indicating that amino acids play an essential role in initiating mTORC1 activity by translocation of mTOR to the lysosomes.

Finally, we used confocal microscopy to assess the consequences of BCH and rapamycin treatment on the asymmetric translocation of mTOR to the lysosome in dividing $CD8^+$ T cell pairs. While untreated dividing $CD8^+$ T cells showed punctate and asymmetric localization of mTOR to the lysosome (Fig. 5g), treatment with BCH resulted in a dispersed distribution of mTOR throughout the cytoplasm in both daughter cells, indicating abrogated mTOR translocation to the lysosome (Fig. 5g), whereas rapaymcin-treated daughter T cells showed a similar mTOR distribution as non-treated T cells (Fig. 5g). Overall, these data suggest that the asymmetric partitioning of CD98 regulates the leucine-mediated translocation of mTOR to the lysosomes preferentially in the $CD8^{hi}$ $CD98^{hi}$ daughter T cells compared to the $CD8^{lo}$ $CD98^{lo}$ T cells (Supplementary Fig. 5).

Discussion

mTOR has been identified to regulate $CD4^+$ and $CD8^+$ T cell differentiation [7–13,15–17,20]. Upon T cell activation, mTORC1 activity can distinguish $CD4^+$ T cells with distinct fates [12]. Here we show that asymmetric partitioning of mTORC1 activity following initial division of $CD8^+$ T cells leads to the generation of two daughter cells with distinct metabolic programming. The daughter T cell ($CD8^{hi}$) proximal to the APC inherits increased mTORC1 activity and is highly glycolytic, two properties that are required for robust effector cell function [16,17,35,36]. Alternatively, the daughter cell ($CD8^{lo}$) distal to the APC inherits decreased mTORC1 activity and is less glycolytic, but possesses increased mitochondria and SRC, as well as increased expression of anti-apoptotic molecules, and as such, have a metabolic programming similar to that of long-lived memory cells [24,25].

Previous findings have identified two distinct daughter T cells based upon CD8 expression [2]. Based on our observations that link mTORC1 activity and amino acid transporter CD98 to asymmetric division, we propose that tracking the asymmetric partitioning of mTORC1 activity or CD98 represent better, more functional marker of asymmetric division of $CD8^+$ T cells. We also noticed the ability of mTORC1 to enhance MYC expression in $CD8^{hi}$ daughter T cells thereby promoting metabolic reprogramming downstream of mTORC1. Our observations that effector and memory T cell generation are intimately linked to metabolic reprogramming during early $CD8^+$ T cells division underscore the integral role of metabolism in defining immune cell function [19]. Consistent with such a model, a recent report linked PI3K signaling and nutrient sensing to T and B cell fate decisions [6].

Mechanistically, our study links asymmetric mTORC1 activation based on the differential RagC-mediated translocation of mTOR to the lysosomes between dividing daughter $CD8^+$ T cells. Here we document that TCR-induced mTORC1 activation and mTOR lysosomal translocation is dependent on amino acid influx. We observed that the asymmetric partitioning of mTORC1 activity was facilitated by the asymmetric partitioning of TCR-

induced amino acid transporters, which is consistent with the critical role of SLC7A5 in promoting T cell effector function [32]

While our observations are consistent with previous reports demonstrating the generation of effector and memory T as a result of asymmetric division of $CD8^+$ T cells [2,3,21,23], our work does not preclude a model whereby the generation of memory T cells is derived from the effector pool [37–39]. Ultimately, we believe it is the level of mTORC1 activity a $CD8^+$ T cell possesses and the subsequent downstream metabolic programming that influences its fate, thereby potentially integrating into all proposed models. For instance, in our current study, a dividing wild-type $CD8^+$ T cell pair with different levels of mTORC1 activity will result in diverse T cell fate. Supporting this, our previous work proves that T cells with equal levels of high (T-*Tsc2*$^{-/-}$) or low (T-*Rheb*$^{-/-}$) mTORC1 activity will result in one fate at the expense of the other [16]. Asymmetric partitioning of proteins and signaling molecules is thought to play a role in driving divergent cellular functions during differentiation. As such, examining the partitioning of mTORC1 activity in other cell types, tissues or organisms may help elucidate mechanisms of cellular differentiation.

Methods

Mice

Six- to eight-week-old male or female mice were used for performing all the experiments in this study. All mouse procedures were approved by the Johns Hopkins University Institutional Animal Care and Use Committee. C57BL/6, GFPMYC, *Cd4*-Cre and OT-I, *Cd90.1*, *Rag2*$^{-/-}$ mice were obtained from Jackson Laboratories. Mice with *lox*P-flanked *Tsc2* alleles were kindly provided by the laboratory of Dr. Michael Gambello. Mice with *lox*P-flanked *Rheb* alleles were generously gifted from Dr. Paul Worley. No empirical test was performed for choosing sample size prior to experiments. No randomization of samples or animals was used nor were investigators blinded throughout the study.

Antibodies and Reagents

Antibodies against the following proteins were purchased from BD Biosciences: CD8α (53-6.7, 1:500), CD90.1 (OX-7, 1:1000), CD69 (H1.2F3, 1:300), CD90.2 (53-2.1, 1:500), CD25 (PC61, 1:500), CD62L (MEL-14, 1:400), Streptavidin-PerCP (554064, 1:300) and Fc Block (2.4G2, 1:100). Antibodies against CD8β (H35-17.2, 1:500), T-bet (eBio4B10, 1:500), CD44 (IM7, 1:400), CD98 (RL388, 1:500) and Eomes (Dan11mag, 1:400) were purchased from eBioscience. Fc-mICAM-1 Chimera from R&D systems. The following antibodies were purchased from Cell Signaling: TSC2 (D93F12, 1:300), p-TSC2 (S939, 1:300), p-S6 (S240/244, D68F8, 1:1000 for flow cytometry and 1:4000 for immunoblotting), AKT (11E7, 1:2000), p-AKT (S473, D9E, 1:2000), p-4E-BP1 (T37/46, 236B4, 1:300 for flow cytometry and 1:2000 for immunoblotting), mTOR (7C10, 1:300), RagC (D8H5, 1:300), p-ERK(T202/Y204, D13.14.4E, 1:2500), hexokinase 2 (C64G5, 1:1000), MYC (D84C12, 1:1000), GLUT-1 (D3J3A, 1:1000), VDAC (D73D12, 1:2500), SDHA (D6J9M, 1:2500), BCL-2 (D17C4, 1:2500), and BCL-xL (54H6, 1:2500). Anti-LAMP-2 (GL2A7, 1:300), CPT-1α (EPR12740(B), 1:1000), and NDUFB8 (20E9DH10C12, 1:1000) were purchased from Abcam. LaminB (C-20, 1:2000) was purchased from Santa Cruz Biotechnology. Anti-β-

tubulin (AA2, 1:1000), talin (8d4, 1:500), and actin (A2066, 1:4000) was purchased from Sigma. OVA-I peptide (SIINFEKL) was purchased from AnaSpec. Stimulatory anti-CD3 (2C11) and anti-CD28 (37.51) were purified from hybridoma supernatants prepared "in-house." CFSE and non-conjugated CD8α (5H10, 1:300) antibody used for microscopy were obtained from Invitrogen. Cell Proliferation Dye-eFluor450 and fixable viability dye eFluor780 were purchased from eBiosciences. Rapamycin was purchased from LC laboratories. 2-aminobicyclo-(2,2,1)-heptane-2-carboxylic acid (BCH), PMA, and ionomycin were purchased from Sigma Aldrich. Secondary fluorophore conjugated antibodies were purchased from Invitrogen: anti-rabbit Alexa Fluor488, anti-rabbit Alexa Fluor647, anti-rabbit Alexa Fluor405, anti-rat Alexa Fluor555, and anti-mouse Alexa Fluor405 (all dilutions in 1:500 to 1:1000). MitoTracker dye was purchased from Invitrogen. All antibody validation profiles can be found via 1DegreeBio (http://1degreebio.org/) or CiteAb (http://www.citeab.com).

T cell *in vitro* Stimulation

In vitro stimulation was performed with plate-bound αCD3 (2μg/ml), mICAM-1/Fc chimera (2μg/ml) and αCD28 (2μg/ml) in indicated experiments. For PMA + Ionomycin activation, cells are stimulated with PMA (50ng/ml) and Ionomycin (500ng/ml) for 5 h and washed out. Otherwise, splenocytes were stimulated with 5 μg/ml OVA class I peptide (SIINFEKL) for indicated time intervals.

Flow Cytometry & Cell Sorting

All experiments were performed on a BD FACS Calibur, LSR II or Aria II and analyzed using FlowJo software. For all flow cytometry experiments gates were set appropriately with unstimulated T cells.

$CD8^+$ T Cells Adoptive Transfer

For *ex vivo* phenotyping of $CD8^{hi}$ and $CD8^{lo}$ T cells in first division, splenocytes were harvested from OT-I mice and adoptively transferred (i.v.) into congenically mismatched WT hosts. Twenty-four hours post-transfer, mice were infected with WT non-attentuated LM-OVA. Forty-eight hours post-infection, spleens were harvested and processed for subsequent analysis.

For acute and memory experiment, OT-I *Rag2*$^{-/-}$ $CD90.2^+$ splenocytes were stimulated with 5μg/ml OVA-I peptide for 36–40 h and sorted $CD8^{hi}$ and $CD8^{lo}$ T cells from first division. 5×10^4 $CD8^{hi}$ or $CD8^{lo}$ T cells were adoptively transferred (i.v.) into C57BL/6 WT $CD90.1^+$ recipients. Recipient mice were either infected with 1×10^6 plaque-forming units vaccinia-OVA on day 0 or on day 21 post-transfer. Six days after infection (Day 6 or Day 27), spleens were harvested and quantification of $CD90.2^+$ $CD8^+$ T cells was assessed.

Immunoblot Analysis

$CD8^{hi}$ and $CD8^{lo}$ T cells are sorted from first division. Samples were flash frozen and lysed in RIPA lysis buffer with protease and phosphatase inhibitor cocktails. Proteins were detected by ECL Plus substrate (GE Healthcare). All images were obtained using UVP Biospectrum500 Imaging System.

Real Time PCR

T cells were stimulated and sorted as described under T cell *in vitro* stimulation. Total RNA was collected using TRIzol reagent (Life Technologies). cDNA was generated with ProtoScript II RT (New England BioLabs) and Real time PCR was performed using TaqMan Universal Master Mix II (Life Technologies). Real time PCR primers and probes obtained from Applied Biosystems: *Ifng* (Mm99999071_m1), *Prf1* (perforin, Mm00812512_m1), and *Slc7a5* (solute carrier family 7, member 5, Mm00441516_m1). Human18s (Life Technologies) is used as endogenous control.

ELISA

IFN-γ was analyzed by mouse ELISA Ready-SET-Go! kit as recommended by the manufacturer (eBioscience).

Mitochondrial and genomic DNA analysis

Total DNA was isolated from sorted cells using QIAamp DNA kit (QIAGEN) according to the manufacturer's protocol. Isolated DNA were quantified by Nanodrop. Real time PCR was performed using SYBR Green (Life Technologies) according to the manufacturer's protocol. Primers for amplifying genomic DNA and mitochondrial DNA are specific for H19 and Nd1 respectively. H19: Forward 5′-GTACCCACCTGTCGTCC-3′ and Reverse 5′-GTCCACGAGACCAATGACTG-3′. Nd1: Forward 5′-AATCGCCATAGCCTTCCTAACAT-3′ and Reverse 5′-GGCGTCTGCAAATGGTTGTAA-3′.

Metabolic Assays

Preparation of cells as described under T cell *in vitro* stimulation. 1.5×10^5 cells were plated per well on coated TC-treated XF96 cell culture microplate coated with poly-D lysine (50μg/ml). SRC was determined by dividing the maximal OCR (detected following FCCP administration) by the basal OCR. Glycolytic stress test was performed with media containing XF Assay Medium Modified DMEM. Plating media for mitochondrial stress test contained 25mM Glucose, 2mM L-Glutamine, 1mM Na pyruvate in XF Assay Medium Modified DMEM. Experiments were performed using XF 96 Extracellular Flux Analyzer (Seahorse Biosciences). The following were injected at the indicated time interval: D-glucose (5mM), 2-deoxyglucose (2DG, 0.1mM), oligomycin (2μM), FCCP (0.5mM), Rotenone (2μM) and Antimycin A (4μM).

Phospho-Flow Cytometry

$CD8^+$ T cells were surface stained with anti-CD8 biotin (53-6.7, BD Bioscience), fixed with 2% formaldehyde for 15 min in 37°C and permeabilized with ice-cold 90% methanol at −20°C for 20 min. After washing, cells were blocked in 10% FBS solution with Fc Block. Staining was analyzed by flow cytometry.

Imaging APCs and T Cells Interaction

To image antigen presenting cells (APCs) and T cells interaction, APCs were derived from bone marrow cells from femur and tibia of C57BL/6 mice and cultured in the presence of

GM-CSF (10ng/ml) and IL-4 (5ng/ml) for 6 days. On day 3 and 5, new medium supplemented with GM-CSF (10ng/ml) and IL-4 (5ng/ml) was added. On day 6, loosely adherent cells in the culture were harvested, and 7.5×10^4 cells were plated on slides overnight. After incubation with OVA-I peptide (1μg/ml) for 1 h at 37°C. After washing, 2.5×10^4 OT-I $CD8^+$ T cells were overlaid. Cells are activated and fixed at indicated time points.

Confocal Microscopy

$CD8^+$ T cells were activated *in vitro* with plate-bound stimulation for 28–36 h depending on genotypes and experimental treatment. Cells were treated with 10μM Cytochalasin B (Sigma) 2–3 h before fixation. Slides were coated with 50μg/ml Poly-D Lysine (Sigma) overnight and vigorously washed before addition of cells. Cells on slides were fixed with 4% paraformaldehyde (methanol free, Thermo Scientific) for 10 min before washing with PBS. Slides were then permeabilized with 90% methanol or 0.1% Triton X-100 (Sigma) followed by blocking in 5% goat serum (Gibco). Slides were then stained as described in phospho-flow cytometry methods above or in 0.01% Tween-20 (Sigma) in 5% goat serum. Slides were mounted with Slow Fade Gold anti-fade reagent with or without DAPI (Invitrogen). Cells were imaged with either an upright 710NLO-Meta confocal module (AxioExaminer; Zeiss) with a 63× /1.2W C-Apo objective or an inverted 780-Quasar confocal module (AxioObserver; Zeiss) with a 40× /1.2 PlanApo oil objective. Data were acquired with Zen imaging software (Zeiss) and analyzed with either ZEN (Zeiss) or Volocity (PerkinElmer) analysis software. Paired dividing T cells were identified based on the presence of tubulin bridge between conjoined cells or the shape of nucleus by DAPI staining. Molecules are considered to be asymmetrically divided if the ratio of dividing daughter cells exceeds two standard deviations above the ratio of the mean of β-tubulin, as described previously [6]. For quantification of co-localization, Global pearson's coefficient (*r*) was calculated from Volocity.

Statistical Analysis

All graphs were created using GraphPad Prism software, and statistical analysis was performed with GraphPad Prism. Paired cell analysis was assessed by Wilcoxon matched-pairs signed rank test; comparisons between 2 independent groups were assessed by Mann-Whitney *t* tests; comparisons between 3 or more independent groups were assessed by One-Way ANOVA with a Holm-Sidak's multiple comparisons test. A p-value less than 0.05 was considered statistically significant. Error bars represent mean ± standard error of the mean.

Supplementary Material

Refer to Web version on PubMed Central for supplementary material.

Acknowledgments

We thank members of the Powell lab and C. Gamper for critical discussion of the manuscript; B. Smith and T. Stephens for their technical support on microscopy studies; M. Gambello (Emory University) for *Tsc2*^{loxP} mice; and P. Worley (Johns Hopkins University) for *Rheb*^{loxP} mice. This work was supported by NIH grants AI072677 (to J.D.P.), AI77610 (to J.D.P.), AI091481 (to J.D.P.), S10 OD016374 (to the JHUSOM Microscope Facility) and S10 RR024550 (to the JHUSOM Microscope Facility).

References

1. Betschinger J, Knoblich JA. Dare to be different: asymmetric cell division in Drosophila, C. elegans and vertebrates. Curr Biol. 2004; 14:R674–685. S0960982204005986 [pii]. DOI: 10.1016/j.cub.2004.08.017 [PubMed: 15324689]
2. Chang JT, et al. Asymmetric T lymphocyte division in the initiation of adaptive immune responses. Science. 2007; 315:1687–1691. 1139393 [pii]. DOI: 10.1126/science.1139393 [PubMed: 17332376]
3. Chang JT, et al. Asymmetric proteasome segregation as a mechanism for unequal partitioning of the transcription factor T-bet during T lymphocyte division. Immunity. 2011; 34:492–504. DOI: 10.1016/j.immuni.2011.03.017 [PubMed: 21497118]
4. Arsenio J, et al. Early specification of CD8+ T lymphocyte fates during adaptive immunity revealed by single-cell gene-expression analyses. Nature immunology. 2014; 15:365–372. DOI: 10.1038/ni.2842 [PubMed: 24584088]
5. Oliaro J, et al. Asymmetric cell division of T cells upon antigen presentation uses multiple conserved mechanisms. Journal of immunology. 2010; 185:367–375. DOI: 10.4049/jimmunol.0903627
6. Lin WH, et al. Asymmetric PI3K Signaling Driving Developmental and Regenerative Cell Fate Bifurcation. Cell Rep. 2015; 13:2203–2218. DOI: 10.1016/j.celrep.2015.10.072 [PubMed: 26628372]
7. Delgoffe GM, et al. The mTOR kinase differentially regulates effector and regulatory T cell lineage commitment. Immunity. 2009; 30:832–844. S1074-7613(09)00237-4 [pii]. DOI: 10.1016/j.immuni.2009.04.014 [PubMed: 19538929]
8. Delgoffe GM, et al. The kinase mTOR regulates the differentiation of helper T cells through the selective activation of signaling by mTORC1 and mTORC2. Nature immunology. 2011; 12:295–303. DOI: 10.1038/ni.2005 [PubMed: 21358638]
9. Lee K, et al. Mammalian target of rapamycin protein complex 2 regulates differentiation of Th1 and Th2 cell subsets via distinct signaling pathways. Immunity. 2010; 32:743–753. S1074-7613(10)00205-0 [pii]. DOI: 10.1016/j.immuni.2010.06.002 [PubMed: 20620941]
10. Heikamp EB, et al. The AGC kinase SGK1 regulates TH1 and TH2 differentiation downstream of the mTORC2 complex. Nature immunology. 2014; 15:457–464. DOI: 10.1038/ni.2867 [PubMed: 24705297]
11. Yang K, et al. T cell exit from quiescence and differentiation into Th2 cells depend on Raptor-mTORC1-mediated metabolic reprogramming. Immunity. 2013; 39:1043–1056. DOI: 10.1016/j.immuni.2013.09.015 [PubMed: 24315998]
12. Pollizzi KN, Waickman AT, Patel CH, Sun IH, Powell JD. Cellular Size as a Means of Tracking mTOR Activity and Cell Fate of CD4+ T Cells upon Antigen Recognition. PloS one. 2015; 10:e0121710. [PubMed: 25849206]
13. Araki K, et al. mTOR regulates memory CD8 T-cell differentiation. Nature. 2009; 460:108–112. [PubMed: 19543266]
14. Pearce EL, et al. Enhancing CD8 T-cell memory by modulating fatty acid metabolism. Nature. 2009; 460:103–107. nature08097 [pii]. DOI: 10.1038/nature08097 [PubMed: 19494812]
15. Rao RR, Li Q, Odunsi K, Shrikant PA. The mTOR kinase determines effector versus memory CD8+ T cell fate by regulating the expression of transcription factors T-bet and Eomesodermin. Immunity. 2010; 32:67–78. [PubMed: 20060330]
16. Pollizzi KN, et al. mTORC1 and mTORC2 selectively regulate CD8(+) T cell differentiation. J Clin Invest. 2015; 125:2090–2108. DOI: 10.1172/JCI77746 [PubMed: 25893604]
17. Finlay DK, et al. PDK1 regulation of mTOR and hypoxia-inducible factor 1 integrate metabolism and migration of CD8+ T cells. J Exp Med. 2012; 209:2441–2453. DOI: 10.1084/jem.20112607 [PubMed: 23183047]
18. MacIver NJ, Michalek RD, Rathmell JC. Metabolic regulation of T lymphocytes. Annu Rev Immunol. 2013; 31:259–283. DOI: 10.1146/annurev-immunol-032712-095956 [PubMed: 23298210]

19. Pollizzi KN, Powell JD. Integrating canonical and metabolic signalling programmes in the regulation of T cell responses. Nat Rev Immunol. 2014; 14:435–446. nri3701 [pii]. DOI: 10.1038/nri3701 [PubMed: 24962260]
20. Pollizzi KN, Powell JD. Regulation of T cells by mTOR: the known knowns and the known unknowns. Trends Immunol. 2015; 36:13–20. S1471-4906(14)00209-9 [pii]. DOI: 10.1016/j.it.2014.11.005 [PubMed: 25522665]
21. Metz PJ, et al. Regulation of Asymmetric Division by Atypical Protein Kinase C Influences Early Specification of CD8(+) T Lymphocyte Fates. Sci Rep. 2016; 6:19182. [PubMed: 26765121]
22. Intlekofer AM, et al. Effector and memory CD8+ T cell fate coupled by T-bet and eomesodermin. Nature immunology. 2005; 6:1236–1244. DOI: 10.1038/ni1268 [PubMed: 16273099]
23. King CG, et al. T cell affinity regulates asymmetric division, effector cell differentiation, and tissue pathology. Immunity. 2012; 37:709–720. DOI: 10.1016/j.immuni.2012.06.021 [PubMed: 23084359]
24. van der Windt GJ, et al. Mitochondrial respiratory capacity is a critical regulator of CD8+ T cell memory development. Immunity. 2012; 36:68–78. DOI: 10.1016/j.immuni.2011.12.007 [PubMed: 22206904]
25. van der Windt GJ, et al. CD8 memory T cells have a bioenergetic advantage that underlies their rapid recall ability. Proc Natl Acad Sci U S A. 2013; 110:14336–14341. DOI: 10.1073/pnas.1221740110 [PubMed: 23940348]
26. Wang R, et al. The Transcription Factor Myc Controls Metabolic Reprogramming upon T Lymphocyte Activation. Immunity. 2011; 35:871–882. S1074-7613(11)00515-2 [pii]. DOI: 10.1016/j.immuni.2011.09.021 [PubMed: 22195744]
27. Gera JF, et al. AKT activity determines sensitivity to mammalian target of rapamycin (mTOR) inhibitors by regulating cyclin D1 and c-myc expression. J Biol Chem. 2004; 279:2737–2746. DOI: 10.1074/jbc.M309999200 [PubMed: 14576155]
28. West MJ, Stoneley M, Willis AE. Translational induction of the c-myc oncogene via activation of the FRAP/TOR signalling pathway. Oncogene. 1998; 17:769–780. DOI: 10.1038/sj.onc.1201990 [PubMed: 9715279]
29. Sancak Y, et al. Ragulator-Rag complex targets mTORC1 to the lysosomal surface and is necessary for its activation by amino acids. Cell. 2010; 141:290–303. DOI: 10.1016/j.cell.2010.02.024 [PubMed: 20381137]
30. Zoncu R, et al. mTORC1 senses lysosomal amino acids through an inside-out mechanism that requires the vacuolar H(+)-ATPase. Science. 2011; 334:678–683. 334/6056/678 [pii]. DOI: 10.1126/science.1207056 [PubMed: 22053050]
31. Bar-Peled L, Schweitzer LD, Zoncu R, Sabatini DM. Ragulator is a GEF for the rag GTPases that signal amino acid levels to mTORC1. Cell. 2012; 150:1196–1208. S0092-8674(12)00998-1 [pii]. DOI: 10.1016/j.cell.2012.07.032 [PubMed: 22980980]
32. Sinclair LV, et al. Control of amino-acid transport by antigen receptors coordinates the metabolic reprogramming essential for T cell differentiation. Nature immunology. 2013; 14:500–508. DOI: 10.1038/ni.2556 [PubMed: 23525088]
33. Torrents D, et al. Identification and characterization of a membrane protein (y+L amino acid transporter-1) that associates with 4F2hc to encode the amino acid transport activity y+L. A candidate gene for lysinuric protein intolerance. J Biol Chem. 1998; 273:32437–32445. [PubMed: 9829974]
34. Liu X, Charrier L, Gewirtz A, Sitaraman S, Merlin D. CD98 and intracellular adhesion molecule I regulate the activity of amino acid transporter LAT-2 in polarized intestinal epithelia. J Biol Chem. 2003; 278:23672–23677. DOI: 10.1074/jbc.M302777200 [PubMed: 12716892]
35. Chang CH, et al. Posttranscriptional control of T cell effector function by aerobic glycolysis. Cell. 2013; 153:1239–1251. DOI: 10.1016/j.cell.2013.05.016 [PubMed: 23746840]
36. Sukumar M, et al. Inhibiting glycolytic metabolism enhances CD8+ T cell memory and antitumor function. J Clin Invest. 2013; 123:4479–4488. DOI: 10.1172/JCI69589 [PubMed: 24091329]
37. Bannard O, Kraman M, Fearon DT. Secondary replicative function of CD8+ T cells that had developed an effector phenotype. Science. 2009; 323:505–509. DOI: 10.1126/science.1166831 [PubMed: 19164749]

38. Wherry EJ, et al. Lineage relationship and protective immunity of memory CD8 T cell subsets. Nature immunology. 2003; 4:225–234. DOI: 10.1038/ni889 [PubMed: 12563257]

39. Kaech SM, Cui W. Transcriptional control of effector and memory CD8+ T cell differentiation. Nat Rev Immunol. 2012; 12:749–761. DOI: 10.1038/nri3307 [PubMed: 23080391]

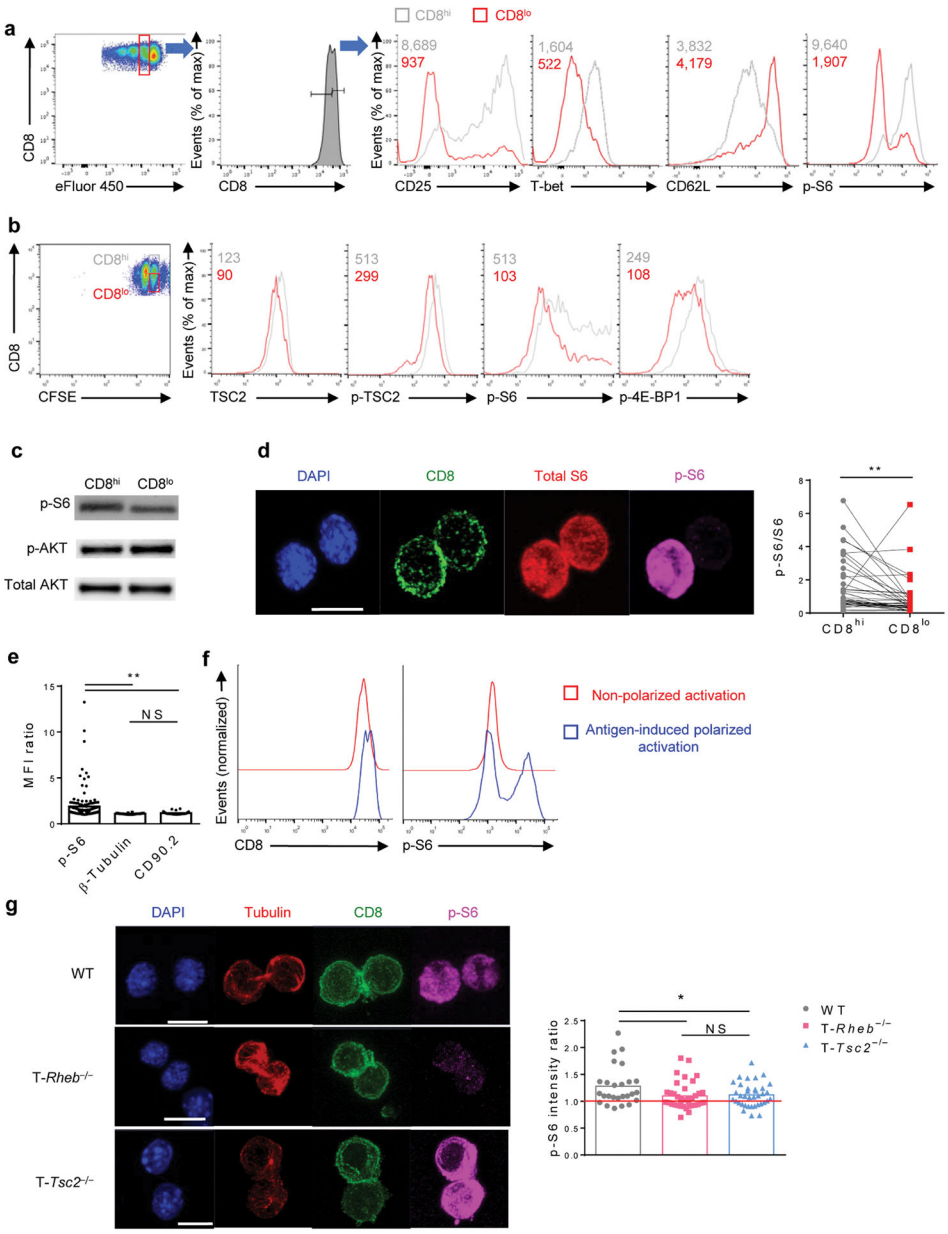

Figure 1. mTORC1 activity is asymmetrically inherited in dividing CD8$^+$ T cells upon TCR stimulation

(**a**) Flow cytometry analyzing adoptive transferred CD8^{hi} and CD8^{lo} eFluor450-labeled OT-I T cells gated on the first division from splenocytes of WT host mice at 48 h post LM-OVA infection. Histogram overlay of CD25, T-bet, CD62L, and p-S6 expression between CD8^{hi} and CD8^{lo} T cells. MFI, upper left corner. (**b**) Histogram overlay of mTOR pathway proteins between CFSE-labeled CD8^{hi} and CD8^{lo} T cells (gated as shown) that were stimulated *in vitro* for 36 h. MFI, upper left corner. (**c**) Immunoblot analysis of mTOR substrates of sorted *in vitro* activated CD8$^+$ T cells. (**d**) Confocal images of dividing T cells that were activated *in vitro*. Quantification of the ratio of phosphorylated to total MFI of S6, n=39. (**e**) Quantification of MFI ratio of p-S6, β-tubulin, and CD90.2among dividing daughter pairs,

n=132 (p-S6), 26 (β-tubulin and CD90.2). (**f**) Histogram overlay of CD8 and p-S6 expression from first-division adoptive transferred OT-I $CD8^+$ T cells into either *Rag2*$^{-/-}$ or LM-OVA infected WT host. (**g**) Confocal images of *in vitro* stimulated WT, T-*Rheb*$^{-/-}$, and T-*Tsc2*$^{-/-}$ $CD8^+$ daughter T cells. Statistics analysis of p-S6 MFI ratio between $CD8^{hi}$ and $CD8^{lo}$ daughter T cells, n=26 (WT) and 37 (T-*Rheb*$^{-/-}$ and T-*Tsc2*$^{-/-}$). **P* < 0.05; ***P* < 0.0001; NS, not significant (Wilcoxon rank test (**d**) or One-way ANOVA (**e, g**)). Data are compiled from 3 independent experiments (**d, e**) or one experiment representative of at least 3 independent experiments (**a–c, f, g**) (mean in **e, g**). Scale bars, 10μm (**d, g**).

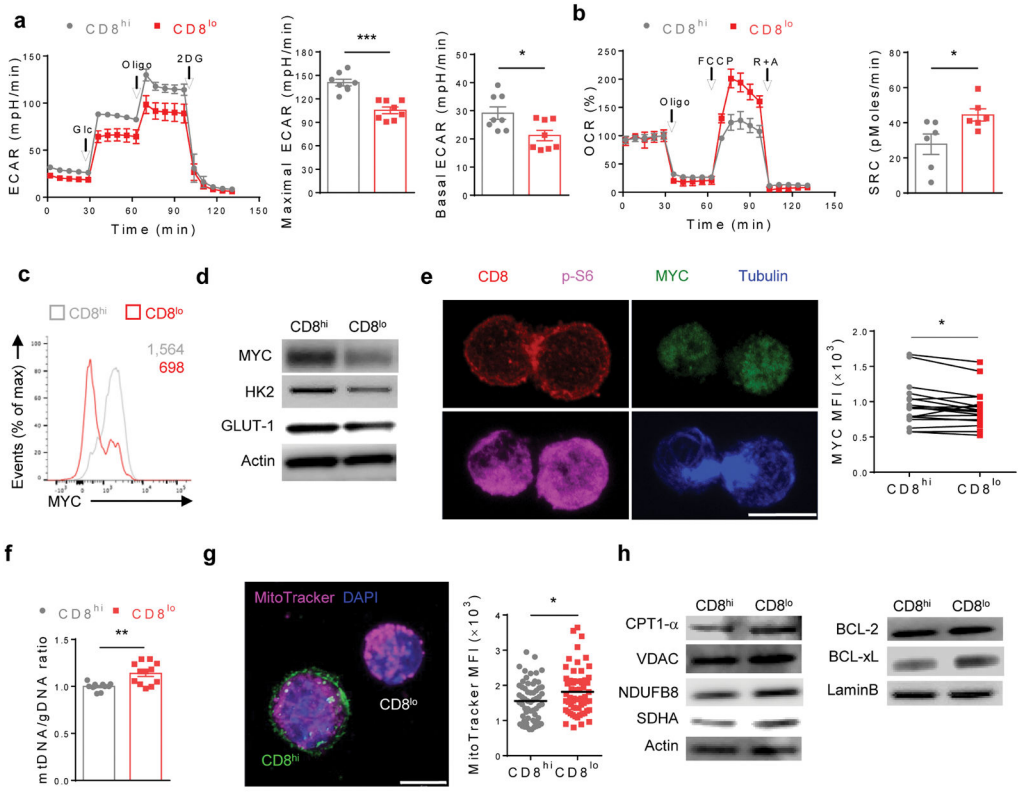

Figure 2. Asymmetric inheritance of mTORC1 results in CD8$^+$ T daughter cells with distinct metabolic capabilities

(**a–b**) CD8^{hi} and CD8^{lo} T cells from *in vitro* activation were assayed for ECAR (**a**) and OCR (**b**). Summary of basal ECAR, maximum ECAR, and SRC are shown on right, n=8 (**a**), 6 (**b**). (**c**) As in Fig. 1a, Histogram overlay showing MYC expression between CD8^{hi} and CD8^{lo} T cells. MFI, upper right corner. (**d**) Immunoblot analysis comparing expression of proteins involved in glycolytic pathway between *in vitro* stimulated CD8^{hi} and CD8^{lo} T cells. (**e**) Confocal images of *in vitro* stimulated daughter CD8$^+$ T cells from GFPMYC mice stained with CD8 and p-S6. Statistical analysis of GFPMYC MFI between CD8^{hi} and CD8^{lo} T cells (right), n=18. (**f**) Quantification of mitochondrial and genomic DNA ratio between sorted *in vitro* activated CD8^{hi} and CD8^{lo} T cells, n=12. (**g**) Immunoblot analysis showing expression of mitochondrial associated proteins comparing between CD8^{hi} and CD8^{lo} T cells as in (**d**). (**h**) Confocal images of *in vitro* activated CD8^{hi} and CD8^{lo} T cells stained with MitoTracker dye and DAPI. CD8^{hi} T cells (green) are further stained with a different CD8 antibody clone post-sort to distinguish between CD8^{lo} T cells. Statistical analysis of MitoTracker MFI between CD8^{hi} and CD8^{lo} cells, n=60. *$P < 0.05$; **$P < 0.005$; ***$P <$ 0.0005 (Mann-Whitney *t* test (**a, b, f, h**) or Wilcoxon rank test (**e**)). Data are from one experiment representative of at least 3 independent experiments (**a–e, g**) or compilation of 3 independent experiments (**f**) (mean ± s.d. in **a, b** left, mean ± s.e.m. in **a, b, f**). Scale bars, 10μm (**e, h**).

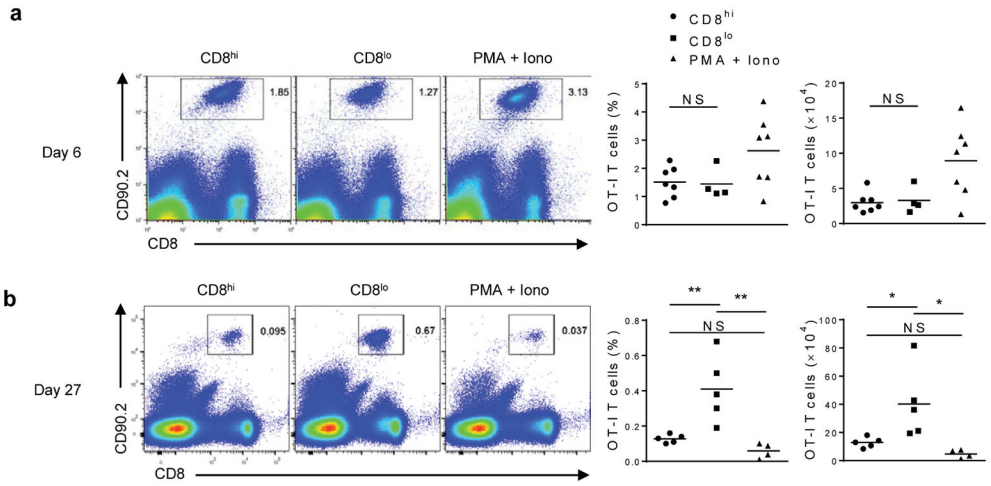

Figure 3. Asymmetric inheritance of mTORC1 results in CD8$^+$ T daughter cells with different *in vivo* survival

PMA + Ionomycin-activated or sorted CD8^{hi} and CD8^{lo} T cells from *in vitro* activation were adoptively transferred into congenically distinct WT host, and then were infected with vaccinia-OVA the same day (**a**) or 21 days later (**b**). Six days after infection (day 6 or day 27), spleens were harvested and quantification of CD90.2$^+$ CD8$^+$ T cells was assessed by flow cytometry. Statistical quantification of percentage and absolute number of recovered CD90.2$^+$ CD8$^+$ T cells between CD8^{hi}, CD8^{lo}, and PMA + Iono activated T cells 6 days or 27 days after the adoptive transfer (six days after infection) are shown, n= 7,4,7 (**a**, CD8^{hi}, CD8^{lo}, PMA+Iono), 5,5,4 (**b**, CD8^{hi}, CD8^{lo}, PMA+Iono). *$P < 0.05$; **$P < 0.005$; NS, not significant (One-Way ANOVA). Data are from one experiment representative of at least 4 independent experiments (mean).

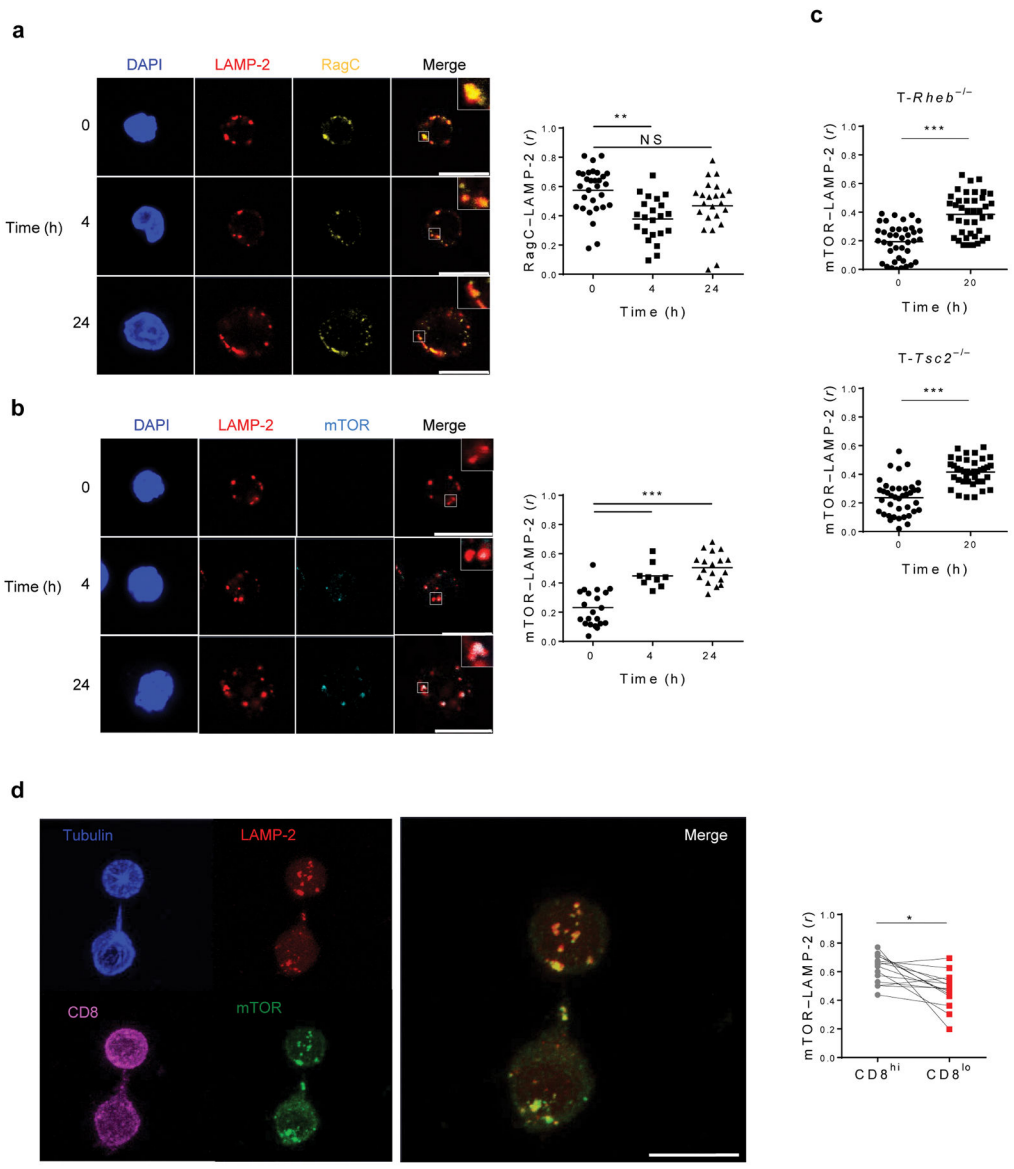

Figure 4. The differential RagC mediated translocation of mTOR to the lysosome contributes to the asymmetric division of CD8$^+$ T cells

(**a**) OT-I *Rag2*$^{-/-}$ splenocytes were stimulated *in vitro* with OVA-I peptide for 0, 4, or 24 h. RagC and LAMP-2 localization was assessed by confocal microscopy. Statistical analysis of co-localization of RagC and LAMP-2 (*r*) was assessed, n=30, 22, 23 (0, 4, 24 h). (**b**) Same as (**a**), except co-localization analysis for mTOR and LAMP-2, n=22, 9, 18 (0, 4, 24 h). (**c**) Statistical analysis of co-localization of mTOR and LAMP-2 (*r*) in CD8$^+$ T cells from T-*Rheb*$^{-/-}$ and T-*Tsc2*$^{-/-}$ at indicated time point after TCR activation, n=40 (T-*Rheb*$^{-/-}$), 39 (T-*Tsc2*$^{-/-}$). (**d**) Confocal images of *in vitro* activated CD8$^+$ T cells showing localization of LAMP-2 and mTOR between CD8^{hi} and CD8^{lo} daughter T cells. Statistical analysis of co-localization of mTOR and LAMP-2 (*r*) between paired daughter cells are shown on the right, n=14. *P < 0.005; **P < 0.0005; ***P < 0.0001; NS, not significant (One-Way ANOVA (**a, b**), One-Way ANOVA (**c**) or Wilcoxon rank test (**d**)). Data are from one experiment

representative of at least 2 independent experiments (mean in **a–c**). Scale bars, 10μm (**a, b, d**).

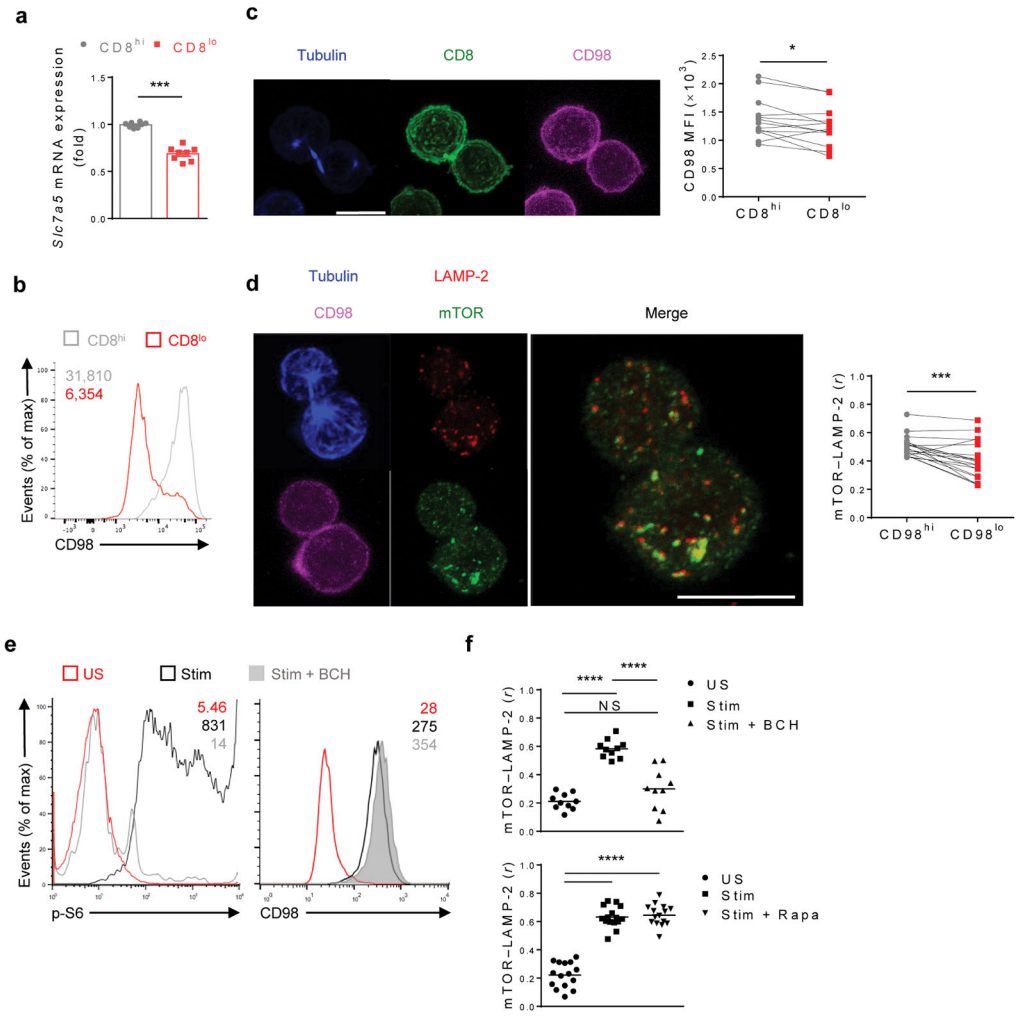

Figure 5a

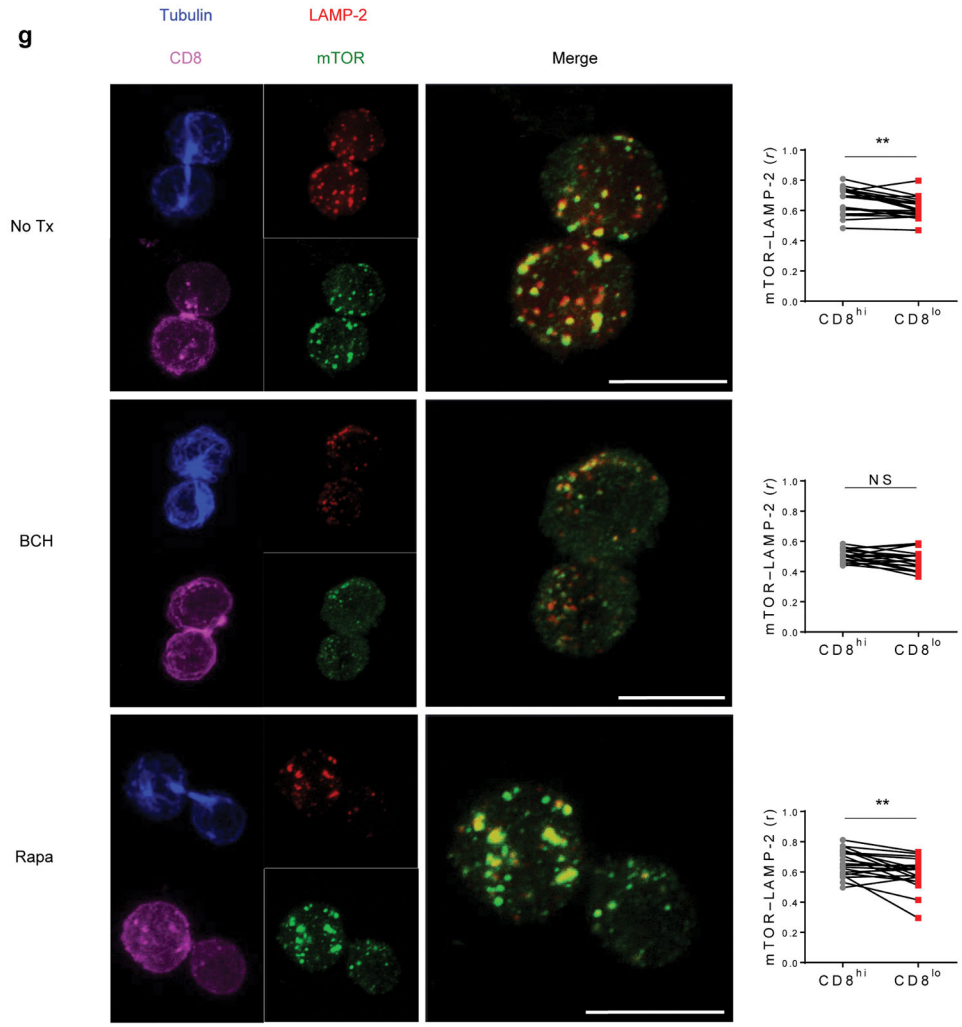

Figure 5b

Figure 5. TCR-induced mTOR localization to lysosome is dependent on differential amino acid transporter expression

(**a**) qRT-PCR analysis of *Slc7a5* mRNA expression in sorted $CD8^{hi}$ and $CD8^{lo}$ T cells activated *in vitro*, n=8. (**b**) As in Fig. 1a, histogram overlay of CD98 expression in $CD8^{hi}$ and $CD8^{lo}$ T cells. MFI, upper left corner. (**c**) Confocal images of CD8 and CD98 expression between daughter cells activated *in vitro*. Statistical analysis of CD98 MFI between $CD8^{hi}$ and $CD8^{lo}$ daughter T cells, n=13. (**d**) Confocal images of mTOR and LAMP-2 localization between daughter $CD8^+$ T cells from *in vitro* activation. Statistical analysis of co-localization of mTOR and LAMP-2 (*r*) between $CD98^{hi}$ and $CD98^{lo}$ $CD8^+$ T cells, n=19. (**e**) Flow cytometry of p-S6 and CD98 expression in $CD8^+$ T cells activated *in vitro* ± amino acid transporter inhibitor (BCH) and unstimulated (US). MFI, upper right corner. (**f**) Statistical analysis of mTOR and LAMP-2 co-localization in $CD8^+$ T cells under US, no treatment, and BCH (top) or rapamycin (bottom) treatment by confocal microscopy, n=10 (BCH), 15 (rapamycin). (**g**) Confocal images of daughter $CD8^+$ T cells showing localization of LAMP-2 and mTOR among no treatment, BCH, and rapamycin treatment.

Statistical analysis of mTOR and LAMP-2 co-localization (*r*) is shown on the right, n=20. **P* < 0.05; ***P* < 0.005; ****P* < 0.0005; *****P* < 0.0001; NS, not significant (Mann-Whitney *t* test (**a, b**), Wilcoxon rank test (**c, d, g**) or One-Way ANOVA (**f**)). Data are from compilation of 3 independent experiments (**a**), one experiment representative of at least 3 independent experiments (**b–g**) (mean ± s.e.m. in **a**, mean in **f**). Scale bars, 10μm (**c, d, g**).